Astronomy & Astrophysics manuscript no. kink_polar
April 27, 2023

A Statistical Investigation of Decayless Oscillations in Small-scale Coronal Loops Observed by Solar Orbiter/EUI

Arpit Kumar Shrivastav[1,2,3], Vaibhav Pant[1], David Berghmans[4], Andrei N. Zhukov[4], Tom Van Doorsselaere[5], Elena Petrova[5], Dipankar Banerjee[1,2], Daye Lim[4,5], and Cis Verbeeck[4]

[1] Aryabhatta Research Institute of Observational Sciences, Nainital, India-263002
[2] Indian Institute of Astrophysics, Bangalore, India-560034
[3] Department of Physics, Indian Institute of Science, Bangalore, India-560012
[4] Solar-Terrestrial Centre of Excellence - SIDC, Royal Observatory of Belgium, Ringlaan - 3 - Av. Circulaire, 1180 Brussels, Belgium.
[5] Centre for mathematical Plasma Astrophysics, Mathematics Department, KU Leuven, Celestijnenlaan 200B bus 2400, B-3001 Leuven, Belgium.

Received **; accepted **

ABSTRACT

Decayless kink oscillations are omnipresent in the solar atmosphere and a viable candidate for coronal heating. Though there have been extensive studies of decayless oscillations in coronal loops with a few hundred Mm lengths, the properties of these oscillations in small-scale (∼10 Mm) loops are yet to be explored. In this study, we present the properties of decayless oscillations in small loops embedded in the quiet corona and coronal holes. We use high resolution observations from the Extreme Ultraviolet Imager onboard Solar Orbiter with pixel scales of 210 km and 5 s cadence or better. We find 42 oscillations in 33 coronal loops with loop lengths varying between 3 to 23 Mm. The average displacement amplitude is found to be 136 km. The oscillations period has a range of 27 to 276 s, and the velocity amplitudes range from 2.2 to 19.3 km s^{-1}. The observed kink speeds are lower than those observed in active region coronal loops. The variation of loop length with the period does not indicate a strong correlation. Coronal seismology technique indicated an average magnetic field value of 2.1 G. We estimate the energy flux with a broad range of 0.6-314 W m^{-2}. Moreover, we note that the short-period decayless oscillations are not prevalent in the quiet Sun and coronal holes. Therefore, our study suggests that decayless oscillations in small-scale coronal loops are unlikely to provide enough energy to heat the quiet Sun and accelerate solar wind in the coronal holes.

Key words. magnetohydrodynamics (MHD) – Sun: corona – Sun: magnetic fields – Sun: oscillations

1. INTRODUCTION

The outer layers of the solar atmosphere maintain temperatures greater than the solar photosphere. To maintain a million-degree temperature of the solar corona, heating should balance the strong radiative losses. The energy flux needed to equipoise the energy losses in the quiet-Sun, coronal holes, and active region is ∼300 W m^{-2}, ∼800 W m^{-2}, 10^4 W m^{-2}, respectively (Withbroe & Noyes 1977). One of the proposed heating mechanisms of energy transfer in the solar atmosphere is Magnetohydrodynamic (MHD) waves (De Moortel & Browning 2015; Arregui 2015; Van Doorsselaere et al. 2020; Banerjee et al. 2021). The transverse displacements of coronal loops in extreme-ultraviolet (EUV) images are interpreted as the standing kink mode of MHD waves (Schrijver et al. 1999; Aschwanden et al. 1999). Since kink oscillations are ubiquitous in the solar atmosphere (Anfinogentov et al. 2015), they are possible candidates for coronal heating (Van Doorsselaere et al. 2020). The standing kink oscillations have been characterised based on the evolution of oscillation amplitude. The amplitude of oscillations, excited by low coronal eruptions such as jets, flares, and coronal mass ejections (Nakariakov et al. 1999; White & Verwichte 2012a; Goddard et al. 2016; Sarkar et al. 2016), decay with time and are defined as decaying oscillations. Many active-region loops have been observed to oscillate with no apparent decay in amplitude for a few periods, known as decayless oscillations (Tian et al. 2012; Wang et al. 2012; Anfinogentov et al. 2013; Zhong et al. 2022a). The generation of decayless oscillations is a subject of ongoing debate, but evidence from modeling and numerical simulations suggest that these oscillations can be triggered by quasi-steady flows acting as footpoint drivers (Nakariakov et al. 2016; Karampelas & Van Doorsselaere 2020). Furthermore, the excitation of these oscillations due to periodic footpoint drivers has been explored in numerical simulations (Karampelas et al. 2017, 2019; Guo et al. 2019; Shi et al. 2021). Recently, Karampelas & Van Doorsselaere (2021) investigated the origin of decayless waves through vortex shedding, while Afanasyev et al. (2020) demonstrated that the observational signature of decayless oscillations could also be reproduced by random footpoint driving. The decaying and decayless kink oscillations have been extensively studied for the active region and quiescent loops with lengths of a few hundred Mm (for a detailed review on kink oscillations, please see Nakariakov et al. 2021).

In the past, several attempts have been made to investigate whether or not transverse waves carry sufficient energy to heat different regions of the solar atmosphere. Several studies have reported the existence of transverse waves in the solar atmosphere and estimated the energy fluxes by measuring the nonthermal line broadening of the transition region and coronal emission lines (Hassler et al. 1990; Banerjee et al. 1998; Hahn & Savin

Table 1. Datasets used in this study.

Date	Time Interval of observation (UT)	Distance from the Sun (a.u)	Stonyhurst heliographic longitude (deg)	Plate scale (km)	Cadence (s)	Field of view (Mm^2)
2021-09-14	04:08 - 04:26	0.59	-47	210	5	430×430
2021-09-14	05:53 - 06:11	0.59	-47	210	5	430×430
2022-03-30	04:30 - 04:59	0.33	93	119	3	244×244

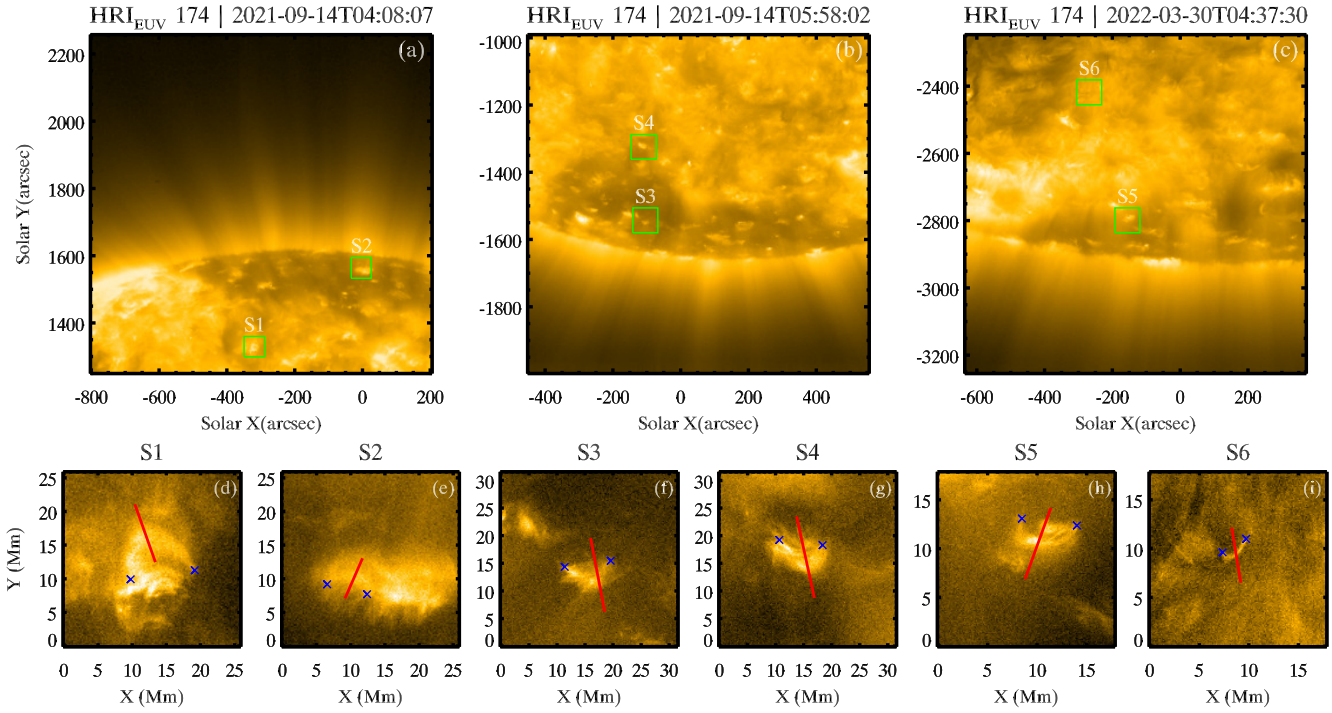

Fig. 1. Description of events. Panel (a),(b), and (c) represents the context images of three datasets used in this study. The green boxes show examples of the selected loops for which oscillations are detected. The other loops examined in this study appear at different times and are not shown here. The magnified view of loops in the green boxes for each upper panel is shown in the lower panels. The red lines in panels (d)-(i) depict the position of artificial slits used to generate distance-time (x-t) maps. The blue crosses in each panel show the approximate position of footpoints. The details of the dataset are provided in table 1. An animation related to this figure is accessible online

2013). These authors advocated that the energy fluxes estimated using the nonthermal line widths are sufficient to heat the solar corona and accelerate solar wind (Hassler et al. 1990; Banerjee et al. 1998; Hahn & Savin 2013). The Doppler velocity fluctuations, which are direct signatures of transverse waves, observed from the Coronal Multi-Channel Polarimeter (CoMP; Tomczyk et al. 2008) were found to be surprisingly small, which indicated that these waves do not provide sufficient energy to heat the active regions (Tomczyk et al. 2007). It was later found that the large line-of-sight integration in the CoMP data leads to the underestimation of wave amplitudes estimated using Doppler velocity fluctuations (McIntosh & De Pontieu 2012; Pant et al. 2019).

The observations of the chromosphere and transition region reveal the omnipresence of kink waves with significant energies to support the energy losses (De Pontieu et al. 2007; Morton et al. 2012; Tian et al. 2014). The High Resolution Coronal Imager (Hi-C; Kobayashi et al. 2014) observations of active-region indicated low energy in coronal loops to support heating (Morton & McLaughlin 2013). The study of transverse motions in fine-scale structures in active region moss revealed that kink waves have larger energy in the lower layers of the atmosphere than in the corona (Morton & McLaughlin 2014). These fine-scale structures were not well resolved by *Atmospheric Imaging Assembly* (AIA; Lemen et al. 2012) on board Solar Dynamic Observatory (SDO; Pesnell et al. 2012). MHD waves play an important role in accelerating the solar wind. The large-scale structures in coronal holes have been explored widely in this context and seen to exhibit transverse motions (McIntosh et al. 2011; Thurgood et al. 2014; Morton et al. 2015, 2019; Weberg et al. 2020). The energy flux of kink waves in open field structures in coronal holes is computed to be less than required for solar wind acceleration (Thurgood et al. 2014; Morton et al. 2015; Weberg et al. 2018).

Quiet-Sun and coronal holes, when seen in X-ray and EUV images, are permeated by small-scale loops and coronal bright points (CBPs) (Golub et al. 1976; Alipour & Safari 2015). Recently, Gao et al. (2022) analysed decayless kink oscillations in CBPs using AIA. The study indicated that decayless oscillations are common in CBPs. The average loop length in their study was ~23 Mm. The resolution of AIA does not allow to detect

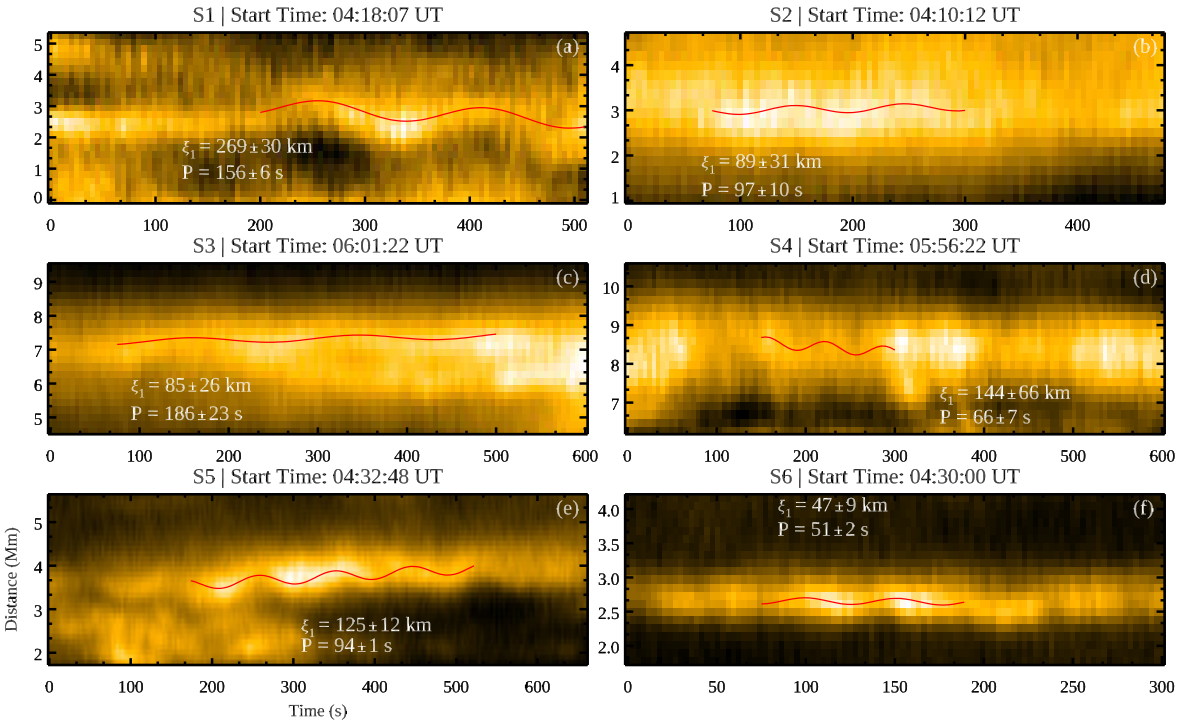

Fig. 2. Overview of x-t maps. Panels (a)-(f) show the x-t maps produced for slits S1 to S6 indicated in Figure 1(d)-(i). The red curves depict the best fit for oscillations. The amplitude, ξ_1, and period, P, of oscillation, along with propagated errors, are written close to fitted oscillations. Few x-t maps show only part of the slits for better visibility of oscillations.

the low-amplitude transverse oscillations in CBPs, so the motion magnification technique was applied to enhance the oscillations. Their study showed that the energy flux in MHD waves in CBPs is not enough to support the radiative losses.

The high resolution and cadence of the Extreme Ultraviolet Imager (EUI; Rochus et al. 2020) onboard Solar Orbiter (Müller et al. 2020) has enabled us to probe the dynamics of the small-scale coronal loops which have largely unclear signatures in AIA (Mandal et al. 2021a). Petrova et al. (2022) performed a case study of two short-period decayless oscillations in the quiet region using EUI. The estimated loop lengths were ∼5-10 Mm. Though these oscillations were observed in the quiet Sun, the wave energy flux was calculated to be of the order of magnitude to balance even active region energy losses. Li & Long (2022) conducted a statistical analysis of 111 small-scale active region loops with an average length of ∼15 Mm. The analysis identified short periods of oscillations ranging from ∼11 to 185 s, with energy fluxes spanning from ∼7 to 9220 W m^{-2}. Their findings revealed that the median wave energy flux of these oscillations is considerably lower than the energy required to heat the active region corona. Additionally, they found a remarkably strong correlation (Pearson coefficient 0.98) between loop length and period. Although several studies of transverse oscillations in the polar region for large-scale structures exist, the kink waves in small loops rooted in the coronal holes and quiet Sun are not examined extensively. In this letter, we present a statistical investigation of oscillation properties of small coronal loops (order of ∼ 10 Mm) rooted in the coronal holes and quiet regions of the solar corona using high-resolution observations from EUI. The letter is structured as follows: Section 2 presents the datasets analysed in this study. Section 3 describes the technique used. The results and discussions are presented in Section 4 followed by Section 5, which concludes the work.

2. OBSERVATION AND DATA

The observational datasets used in this study are obtained from the High Resolution Imager (HRI_{EUV}) telescope of EUI onboard Solar Orbiter. HRI_{EUV} observes the corona at 174 Å which is attributed to Fe IX and Fe X ions and captures the coronal dynamics of plasma at a temperature of ∼ 1MK. It has a field-of-view (FOV) of ∼ 17′× 17′with a plate scale of 0.492″pixel^{-1}.

The Level 2 images are obtained from the EUI data release 5.0 (Mampaey et al. 2022) and 4.0 (Auchère et al. 2021). The EUI images suffer from spacecraft jitter, which was corrected, and images are aligned by applying the cross-correlation technique as suggested in Mandal et al. (2022).

Figure 1(a)-(c) shows the snapshots of the FOV of the Sun observed by HRI_{EUV} for three different datasets. These snapshots show the presence of many small-scale loops. The green boxes outline the loops where oscillations are observed. These images also show large-scale polar coronal holes and plumes. The data sets are focused on the quiet-Sun and polar regions with cadences suitable for observing short-period kink oscillations. The details of the datasets used for identifying the loops and building the statistics are described in Table 1.

We selected several small-scale loops for our study and found 42 oscillating events in 33 loops. These small-scale loops appear dynamic when investigated using animation, and many loops appear and disappear during the time interval of datasets. The properties of some of these loops are similar to active-region fine-scale loops as they possess drifting motions (Li & Long 2022).

3. ANALYSIS

Figure 1(d)-(i) shows the small-scale loops outlined by green boxes corresponding to upper panels (a),(b), and (c). We place

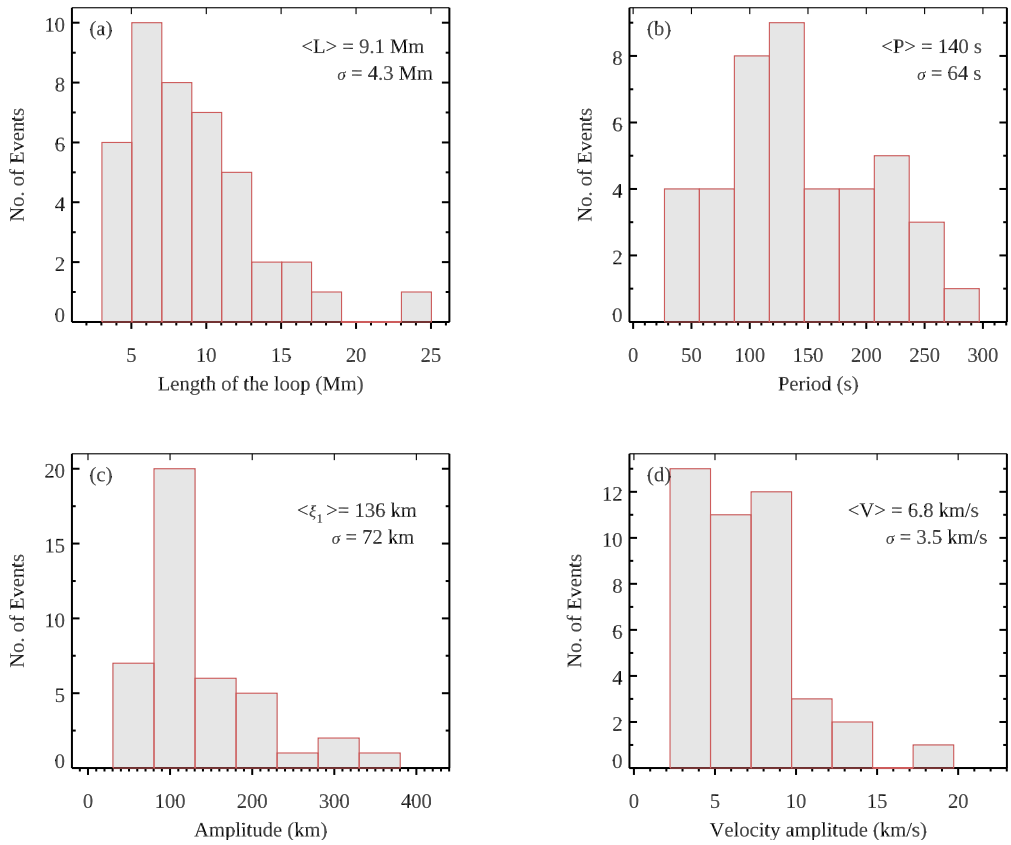

Fig. 3. Distribution of oscillation parameters. The estimated parameter values are displayed as histograms, showcasing the distribution of (a) loop length, (b) period, (c) displacement amplitude, and (d) velocity amplitude. These histograms illustrate the range of values for each parameter, with the average and standard deviation provided in the respective panels.

slits approximately perpendicular to the loop axis, shown by red lines in each panel. These slits are 5 pixels wide and are used for generating distance-time ($x-t$) maps. The intensity is averaged over the width of slits to increase the signal-to-noise ratio (White & Verwichte 2012b; Nisticò et al. 2013).

Figure 2 shows the $x-t$ maps of slits S1 to S6 as displayed in Figure 1(d)-(i). The $x-t$ maps reveal the presence of transverse oscillations. We detected transverse oscillations lasting for 2-6 periods without any decaying signature. These $x-t$ maps indicate only a part of the slit for better visibility of the oscillations. We calculate the uncertainty in the intensity, I, in DN, using the following formula (Petrova et al. 2022),

$$\sigma^2_{\rm DN} = \sigma^2_{\rm readout} + \sigma^2_{\rm photon} \quad (1)$$

$\sigma_{\rm readout}$ denotes the readout noise of the $\rm HRI_{EUV}$ detector, estimated to be 2 DN. Additionally, the variance of photon noise($\sigma^2_{\rm photon}$) is determined by the product of the gain factor, g (with a value of 6.85 DN/photon, Petrova et al. 2022), and the intensity, I. Subsequently, the obtained uncertainty values are employed as errors in intensities to fit a Gaussian function perpendicular to the oscillating structure at each time slice. The Gaussian fitting provides the center of the oscillating structure at a particular time. To obtain the parameter of oscillations, we fit these centers using a sinusoidal function with a linear trend.

$$\xi(t) = \xi_0 + \xi_1 \sin(2\pi t/P + \phi) + \xi_2 t. \quad (2)$$

where ξ_1 represents the oscillation amplitude, P is the period of oscillation, ϕ is phase and ξ_0 and ξ_2 are constants. We implemented the same techniques for calculating oscillation parameters in 42 oscillations, and 6 are shown in Figure 2. The best-fit functions are shown in red curves. The amplitude and period obtained after fitting, along with the values of propagated errors, are indicated in the $x-t$ maps. We haven't used any automatic method to fit the oscillations as performed in previous statistical studies (Thurgood et al. 2014; Weberg et al. 2018, 2020). The velocity amplitude of these oscillations is estimated using the relation $V = 2\pi\xi_1/P$. We compute the uncertainty in velocity amplitude by $\sigma^2_V = \left(\frac{\partial V}{\partial P}\sigma_P\right)^2 + \left(\frac{\partial V}{\partial \xi_1}\sigma_{\xi_1}\right)^2$. The loop length is approximated by measuring the distance between footpoints, assuming the semicircular model of loops. We calculate the loop length using the relation, $L = \pi D/2$, where D is the distance between the footpoints of the loop. We assume the uncertainty in loop lengths to be 40% (discussed in section 4.3).

4. RESULTS AND DISCUSSIONS

4.1. Distribution of Parameters

We estimated the oscillation amplitude, ξ_1, period, P, loop length, L, and velocity amplitude V for oscillations captured using $x-t$ maps and plotted their distribution. Figure 3 shows the histograms of these parameters. The loop lengths vary from 3 to 23 Mm with a mean of 9.1±4.3 Mm. Previous studies of decayless oscillations in active-region loops estimated a few hundred Mm loop lengths (Anfinogentov et al. 2013, 2015). The study of kink oscillations in CBPs estimated loop length in the range of 14-42 Mm (Gao et al. 2022). The loop length of a few loops estimated here overlaps with the recent length measurement of active and quiet region loops using EUI (Petrova et al. 2022; Li & Long 2022). The average loop length in this analysis is shorter

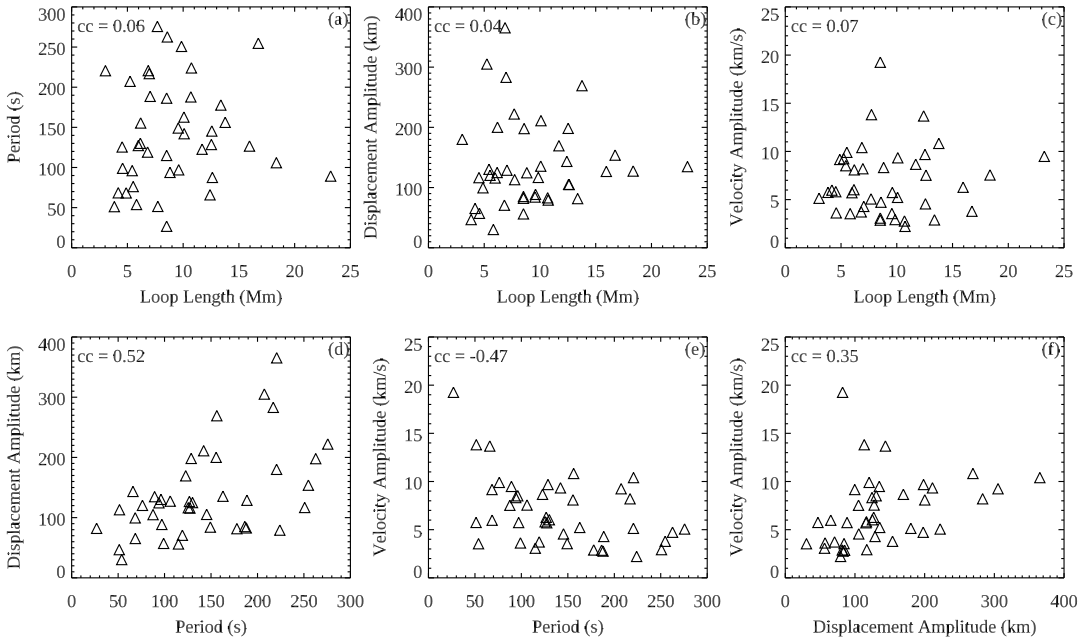

Fig. 4. Relationships between parameters. Panels (a)-(f) show the scatter plots between four estimated parameters, loop length, period, displacement amplitude, and velocity amplitude. The linear Pearson correlation coefficient is also written in each panel.

than in previous statistical studies using AIA due to the high resolution of EUI. The period of oscillations lies between 27 to 276s, with a mean of 140±64s. Around 90% of the oscillations have periods greater than 60s, similar to previously estimated periods for coronal loops (Anfinogentov et al. 2015; Nechaeva et al. 2019; Gao et al. 2022; Zhong et al. 2022b). 10% oscillation periods range from 27 to 60s, analogous to decayless oscillations detected in small loops (Petrova et al. 2022; Li & Long 2022). The displacement amplitudes are in the 31 to 365 km range with an average value of 136±72 km. The displacement amplitude lower than the plate scale of HRI_{EUV} are a result of the fitting procedure. The average displacement amplitude is comparable to the estimated oscillation amplitude in active-region coronal loops (Anfinogentov et al. 2015; Li & Long 2022). In contrast, it is larger than the estimates of amplitudes for coronal bright points (Gao et al. 2022). If we consider a similar amount of energy flux in both scenarios, a greater displacement amplitude is required in smaller loops. The velocity amplitudes are between 2.2 to 19.3 km s^{-1} with a mean of 6.8±3.5 km s^{-1}. The velocity amplitudes found in oscillations in CBPs, active region moss fine structures, and large-scale coronal loops are less than 10 km s^{-1} (Anfinogentov et al. 2013; Morton & McLaughlin 2013, 2014; Nakariakov et al. 2016; Gao et al. 2022) whereas ∼ 15% oscillations in our study have velocity amplitudes larger than 10 km s^{-1}.

4.2. Correlation between different parameters

Figure 4 shows the scatter plots between the estimated parameters, described in section 3. The linear Pearson correlation coefficient is also provided in the plots. The kink speed of an oscillating coronal loop will be proportional to loop length (L) and inverse of the period (P) in long wavelength limit (Edwin & Roberts 1983). So for a close range of kink speeds, the period will be approximately proportional to the loop length as observed in the analysis of decayless oscillations of active-region coronal loops with several hundred Mm lengths (Anfinogentov et al. 2015).

We do not find such a correlation between loop length and the period of oscillations (Figure 4a). Gao et al. (2022) suggested that due to the lower heights of CBPs, a large part of the loops can be embedded in the chromosphere and may result in longer periods. This will also be true for loops with the length of ∼ 10 Mm. The uncertainty in the measurement of loop length (see Van Doorsselaere et al. 2007; Berghmans et al. 2021) could also be a possible reason for the poor correlation. It is also likely that these oscillations could be driven at footpoints and can have periods similar to the driver, resulting in poor correlation as suggested in Gao et al. (2022). Recently, Li & Long (2022) observed short-period oscillations in coronal loops with a mean length of ∼ 15 Mm. They found a suspiciously strong correlation (0.98) between loop length and period. In our study, we find no correlation of loop length with displacement and velocity amplitudes. Moreover, our study indicated a correlation of 0.52 between displacement amplitude and period, as shown in the lower-left panel of Figure 4. It is possible that the correlation between displacement amplitude and period also depends on the sample and, therefore, a selection effect. There may not necessarily be a physical relationship between these two parameters. We find a negative correlation between velocity amplitude and period, as reported in Gao et al. (2022). The positive correlation between displacement and velocity amplitude and the negative correlation between period and velocity amplitude could be due to their direct relationship.

Figure 5 presents the variation of the period with loop length in our work combined with various studies of decayless oscillations compiled from Wang et al. (2012); Nisticò et al. (2013); Anfinogentov et al. (2013, 2015); Duckenfield et al. (2018); Anfinogentov & Nakariakov (2019); Mandal et al. (2021b); Zhong et al. (2022a); Petrova et al. (2022); Zhong et al. (2022b); Gao et al. (2022); Li & Long (2022). The black line provides the least-square fit to these data points with a slope of 1.16±0.05.

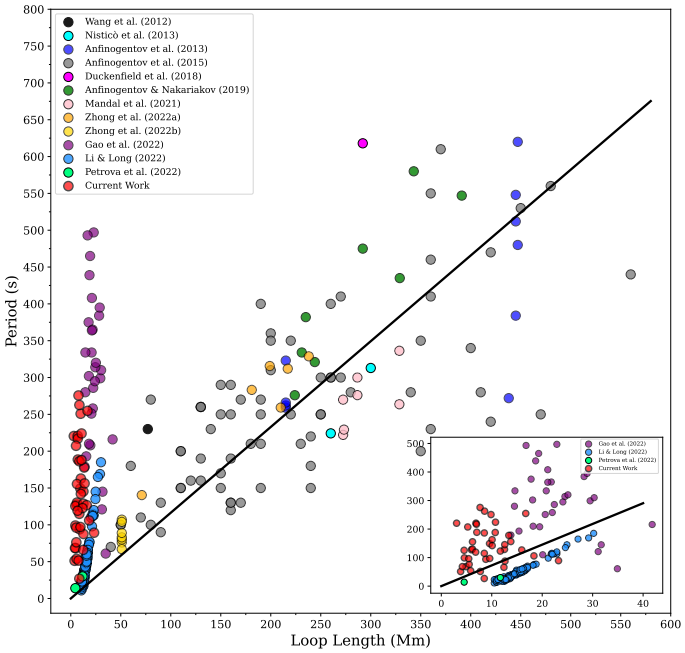

Fig. 5. Scaling between loop length and period. The figure shows the variation of loop length vs. period of decayless oscillations analysed in previous studies (Wang et al. 2012; Nisticò et al. 2013; Anfinogentov et al. 2013, 2015; Duckenfield et al. 2018; Anfinogentov & Nakariakov 2019; Mandal et al. 2021b; Zhong et al. 2022a; Petrova et al. 2022; Zhong et al. 2022b; Gao et al. 2022; Li & Long 2022). The red points represent the results of the current work. The inset plot compares the loop length and period of current work with Gao et al. (2022), Li & Long (2022), and Petrova et al. (2022). The black lines represent the best fit for the data sets.

The small plot in the lower right side compares the variation of loop length with the period of oscillations studied in Gao et al. (2022); Li & Long (2022); Petrova et al. (2022) and this work. The slope of the least-square fitted black line in the inset plot is 7.26±0.45. The red data points are obtained in this study, which shows that the average loop length is shorter than in previous studies. The dependence of oscillation period on loop length suggests the shorter loops will have short periods (Anfinogentov et al. 2015; Goddard et al. 2016; Zhong et al. 2022b; Li & Long 2022). However, several long-period oscillations are observed in CBPs with an average loop length of ~23 Mm (Gao et al. 2022). We also find many oscillations with longer periods in loops of mean length ~10 Mm (see Figure 5). Our analysis suggests that the fraction of high-frequency oscillation is less in quiet Sun and coronal holes compared to active regions, as reported in Li & Long (2022).

4.3. Coronal seismology

In long wavelength limit, the kink speed (C_k) can be calculated as,

$$C_k = \frac{2L}{P}$$

Here we assume that the observed oscillations are fundamental modes. Figure 6(a) shows the distribution of kink speed. The kink speed has a range of 27-635 km s^{-1} with an average of 163±123 km s^{-1}. The estimated kink speed for most loops is less than active region loops (Anfinogentov & Nakariakov 2019) but comparable to kink speeds in CBPs. Using the internal and external intensities ratio, Gao et al. (2022) showed that the internal Alfvén speed is correlated to loop length with a correlation coefficient of 0.63. Although we have not estimated the internal and external intensities, the kink speed and loop length show a correlation of 0.55 in our study. This supports the idea that the Alfvén speed increases with height and will be higher for larger loops.

The magnetic field strength, B, can be estimated using the following relation,

$$B = C_k \sqrt{\mu_0 \rho_i \widetilde{m}} \sqrt{\frac{1+\rho_e/\rho_i}{2}}$$

where ρ_i and ρ_e are the internal and external plasma density, μ_0 and $\widetilde{m}$ denote magnetic permeability in vacuum and mean molecular weight. We take $\rho_i = 10^9 \mathrm{cm}^{-3}$ and density contrast, $\rho_e/\rho_i = 1/3$ for calculating the magnetic field (Gao et al. 2022; Petrova et al. 2022; Li & Long 2022). Figure 6(b) shows the distribution of estimated magnetic field strengths. The average value of the magnetic field is 2.1±1.5 G, with a range of 0.35-8 G. Most of the loops have a magnetic field strength of less than 4 G, which is lower than previous estimates of magnetic field using seismology in a few hundred Mm length loops (Nisticò et al. 2013). The potential field extrapolation of photospheric magnetograms for x-ray bright points shows that several loops with length ~ 10 Mm have magnetic field strength greater than 10 G (Mondal et al. 2023). he magnetic fields obtained in our study are consistent with those in West et al. (2011), who found a magnetic field strength of 0.7±0.7 G in the quiet-Sun region performing coronal seismology using EIT waves. The underestimation of loop length could result in a lower kink speed and, consequently, a small magnetic field strength. The underestimation of loop length can be around 10% for a few hundred Mm loops (Mackay et al. 2000; Van Doorsselaere et al. 2007). The analysis of campfire loops with loop length ~3-4 Mm indicated that this underestimation could increase up to ~ 40-50% as it is possible that the part of the loop, embedded in chromosphere and photosphere is not observed in 174 Å emission (Berghmans et al. 2021). It must be noted that even if we add 50% error in length, the average value of kink speed would be 245 km s^{-1} which remains smaller than those observed in the coronal heights. Since kink speeds depends on the internal and external Alfvén speeds, it might be possible that these structures have quite different density contrasts, and/or magnetic fields compared to large-scale coronal loops. It is important to note that our estimation of magnetic field strengths assumes that the observed oscillations are fundamental modes, which may not necessarily be the case.

4.4. Estimation of energy flux

The energy flux carried by the observed kink waves can be estimated by the following expression (Van Doorsselaere et al. 2014; Petrova et al. 2022):

$$E_f = \frac{1}{2} C_k (\rho_e + \rho_i) V^2.$$

Using the distribution of C_k and V, and considering the values of internal plasma density and density contrast (mentioned in section 4.3), we find a broad range of energy flux, 0.6-314 W m^{-2}. The mean and median of energy flux distribution are 21 and 6 W m^{-2}, respectively. The energy fluxes of 94 and 314 W m^{-2} are obtained for the period of 65 and 27 s with displacement amplitude of ~143 and 82 km. This suggests that short-period

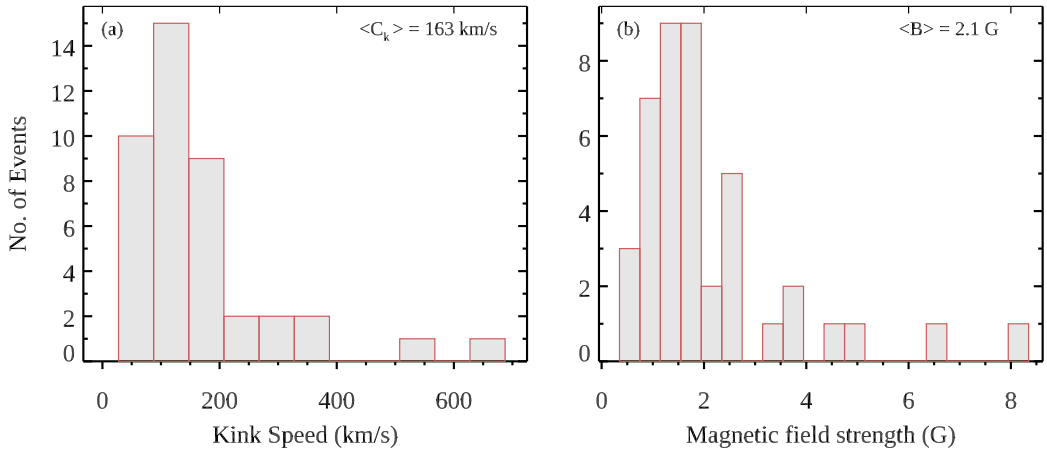

Fig. 6. Results of coronal seismology. The figure shows the histograms of kink speeds, C_k, and magnetic field strength, B, obtained using estimated oscillation parameters. The mean value of the distribution is also provided.

oscillations have high energy flux in the quiet Sun and coronal holes. Petrova et al. (2022) analysed two short-period oscillations of ∼ 14 and 30 s. The wave energy fluxes calculated for these oscillations were 1.9 and 6.5 kW m^{-2}. The analysis showed the existence of short-period high-frequency waves in the quiet Sun region. The study of Gao et al. (2022) presented the long-period low energy decayless waves in bright points. In our study, we find both short-period and long-period oscillations. Figure 5 shows that our study has revealed the existence of periods and loop lengths that were absent in Gao et al. (2022) and Petrova et al. (2022). Though the maximum energy flux, estimated in our study, is sufficient to heat the quiet corona (Withbroe & Noyes 1977), the mean and median energy fluxes indicate that decayless waves with high energy fluxes are not prevalent in quiet Sun and coronal holes.

5. SUMMARY AND CONCLUSION

In this paper, we performed the statistical analysis of decayless kink oscillations in small loops using high resolution observation from HRI$_{EUV}$ telescopes of EUI. The oscillating loops have lengths of the order of 10 Mm, and they are dynamic in nature. The average loop length in this study is shorter than the previous statistical studies of decayless kink oscillations in coronal loops. The analysed loops have mean oscillation period and displacement amplitude of 140s and 136 km, respectively. The estimation of kink speed shows a range of ∼27-635 km s^{-1}, lower than the kink speed found in several hundred Mm loops in active regions. We estimated magnetic field strength using coronal seismology, which indicated lower values than those obtained in active-region loops. The energy flux estimation provided a range of ∼0.6-314 W m^{-2}. We find that the energy flux of most oscillations is insufficient to compensate for radiative losses in the quiet corona and coronal holes. This indicates that transverse oscillations with high energy flux in quiet Sun and coronal holes are not prevalent. In conclusion, the transverse waves in small loops, immersed in coronal holes and quiet corona, do not provide significant energy to balance the radiative losses and accelerate the solar wind.

Acknowledgements. A.K.S is supported by funds of the Council of Scientific & Industrial Research (CSIR), India, under file no. 09/079(2872)/2021-EMR-I. V.P. is supported by SERB start-up research grant (File no. SRG/2022/001687). A.K.S. acknowledges Krishna Prasad Sayamanthula and Ritesh Patel for their thoughtful discussions. A. N. Z. thanks the Belgian Federal Science Policy Office (BELSPO) for the provision of financial support in the framework of the PRODEX Programme of the European Space Agency (ESA) under contract number 4000136424. T.V.D. was supported by the European Research Council (ERC) under the European Union's Horizon 2020 research and innovation programme (grant agreement No 724326), the C1 grant TRACEspace of Internal Funds KU Leuven, and a Senior Research Project (G088021N) of the FWO Vlaanderen. Solar Orbiter is a space mission of international collaboration between ESA and NASA, operated by ESA. The EUI instrument was built by CSL, IAS, MPS, MSSL/UCL, PMOD/WRC, ROB, LCF/IO with funding from the Belgian Federal Science Policy Office (BELSPO/PRODEX PEA 4000112292 and 4000134088); the Centre National d'Etudes Spatiales (CNES); the UK Space Agency (UKSA); the Bundesministerium für Wirtschaft und Energie (BMWi) through the Deutsches Zentrum für Luft- und Raumfahrt (DLR); and the Swiss Space Office (SSO).

References

Afanasyev, A. N., Van Doorsselaere, T., & Nakariakov, V. M. 2020, A&A, 633, L8
Alipour, N. & Safari, H. 2015, ApJ, 807, 175
Anfinogentov, S., Nisticò, G., & Nakariakov, V. M. 2013, A&A, 560, A107
Anfinogentov, S. A. & Nakariakov, V. M. 2019, ApJ, 884, L40
Anfinogentov, S. A., Nakariakov, V. M., & Nisticò, G. 2015, A&A, 583, A136
Arregui, I. 2015, Philosophical Transactions of the Royal Society of London Series A, 373, 20140261
Aschwanden, M. J., Fletcher, L., Schrijver, C. J., & Alexander, D. 1999, ApJ, 520, 880
Auchère, F., Mampaey, B., Verbeeck, F., et al. 2021, SolO/EUI Data Release 4.0 2021-12, https://doi.org/10.24414/s5da-7e78, royal Observatory of Belgium (ROB)
Banerjee, D., Krishna Prasad, S., Pant, V., et al. 2021, Space Sci. Rev., 217, 76
Banerjee, D., Teriaca, L., Doyle, J. G., & Wilhelm, K. 1998, A&A, 339, 208
Berghmans, D., Auchère, F., Long, D. M., et al. 2021, A&A, 656, L4
De Moortel, I. & Browning, P. 2015, Philosophical Transactions of the Royal Society of London Series A, 373, 20140269
De Pontieu, B., McIntosh, S. W., Carlsson, M., et al. 2007, Science, 318, 1574
Duckenfield, T., Anfinogentov, S. A., Pascoe, D. J., & Nakariakov, V. M. 2018, ApJ, 854, L5
Edwin, P. M. & Roberts, B. 1983, Sol. Phys., 88, 179
Gao, Y., Tian, H., Van Doorsselaere, T., & Chen, Y. 2022, ApJ, 930, 55
Goddard, C. R., Nisticò, G., Nakariakov, V. M., & Zimovets, I. V. 2016, A&A, 585, A137
Golub, L., Krieger, A. S., & Vaiana, G. S. 1976, Sol. Phys., 49, 79
Guo, M., Van Doorsselaere, T., Karampelas, K., et al. 2019, ApJ, 870, 55
Hahn, M. & Savin, D. W. 2013, ApJ, 776, 78
Hassler, D. M., Rottman, G. J., Shoub, E. C., & Holzer, T. E. 1990, ApJ, 348, L77

Karampelas, K. & Van Doorsselaere, T. 2020, ApJ, 897, L35
Karampelas, K. & Van Doorsselaere, T. 2021, ApJ, 908, L7
Karampelas, K., Van Doorsselaere, T., & Antolin, P. 2017, A&A, 604, A130
Karampelas, K., Van Doorsselaere, T., Pascoe, D. J., Guo, M., & Antolin, P. 2019, Frontiers in Astronomy and Space Sciences, 6, 38
Kobayashi, K., Cirtain, J., Winebarger, A. R., et al. 2014, Sol. Phys., 289, 4393
Lemen, J. R., Title, A. M., Akin, D. J., et al. 2012, Sol. Phys., 275, 17
Li, D. & Long, D. M. 2022, arXiv e-prints, arXiv:2212.08804
Mackay, D. H., Galsgaard, K., Priest, E. R., & Foley, C. R. 2000, Sol. Phys., 193, 93
Mampaey, B., Verbeeck, F., Stegen, K., et al. 2022, SolO/EUI Data Release 5.0 2022-04, https://doi.org/10.24414/2qfw-tr95, royal Observatory of Belgium (ROB)
Mandal, S., Chitta, L. P., Antolin, P., et al. 2022, A&A, 666, L2
Mandal, S., Peter, H., Chitta, L. P., et al. 2021a, A&A, 656, L16
Mandal, S., Tian, H., & Peter, H. 2021b, A&A, 652, L3
McIntosh, S. W. & De Pontieu, B. 2012, ApJ, 761, 138
McIntosh, S. W., de Pontieu, B., Carlsson, M., et al. 2011, Nature, 475, 477
Mondal, B., Klimchuk, J. A., Vadawale, S. V., et al. 2023, arXiv e-prints, arXiv:2301.02519
Morton, R. J. & McLaughlin, J. A. 2013, A&A, 553, L10
Morton, R. J. & McLaughlin, J. A. 2014, ApJ, 789, 105
Morton, R. J., Tomczyk, S., & Pinto, R. 2015, Nature Communications, 6, 7813
Morton, R. J., Verth, G., Jess, D. B., et al. 2012, Nature Communications, 3, 1315
Morton, R. J., Weberg, M. J., & McLaughlin, J. A. 2019, Nature Astronomy, 3, 223
Müller, D., St. Cyr, O. C., Zouganelis, I., et al. 2020, A&A, 642, A1
Nakariakov, V. M., Anfinogentov, S. A., Antolin, P., et al. 2021, Space Sci. Rev., 217, 73
Nakariakov, V. M., Anfinogentov, S. A., Nisticò, G., & Lee, D. H. 2016, A&A, 591, L5
Nakariakov, V. M., Ofman, L., Deluca, E. E., Roberts, B., & Davila, J. M. 1999, Science, 285, 862
Nechaeva, A., Zimovets, I. V., Nakariakov, V. M., & Goddard, C. R. 2019, ApJS, 241, 31
Nisticò, G., Nakariakov, V. M., & Verwichte, E. 2013, A&A, 552, A57
Pant, V., Magyar, N., Van Doorsselaere, T., & Morton, R. J. 2019, ApJ, 881, 95
Pesnell, W. D., Thompson, B. J., & Chamberlin, P. C. 2012, Sol. Phys., 275, 3
Petrova, E., Magyar, N., Van Doorsselaere, T., & Berghmans, D. 2022, arXiv e-prints, arXiv:2205.05319
Rochus, P., Auchère, F., Berghmans, D., et al. 2020, A&A, 642, A8
Sarkar, S., Pant, V., Srivastava, A. K., & Banerjee, D. 2016, Sol. Phys., 291, 3269
Schrijver, C. J., Title, A. M., Berger, T. E., et al. 1999, Sol. Phys., 187, 261
Shi, M., Van Doorsselaere, T., Guo, M., et al. 2021, ApJ, 908, 233
Thurgood, J. O., Morton, R. J., & McLaughlin, J. A. 2014, ApJ, 790, L2
Tian, H., DeLuca, E. E., Cranmer, S. R., et al. 2014, Science, 346, 1255711
Tian, H., McIntosh, S. W., Wang, T., et al. 2012, ApJ, 759, 144
Tomczyk, S., Card, G. L., Darnell, T., et al. 2008, Sol. Phys., 247, 411
Tomczyk, S., McIntosh, S. W., Keil, S. L., et al. 2007, Science, 317, 1192
Van Doorsselaere, T., Andries, J., & Poedts, S. 2007, A&A, 471, 311
Van Doorsselaere, T., Gijsen, S. E., Andries, J., & Verth, G. 2014, ApJ, 795, 18
Van Doorsselaere, T., Srivastava, A. K., Antolin, P., et al. 2020, Space Sci. Rev., 216, 140
Wang, T., Ofman, L., Davila, J. M., & Su, Y. 2012, ApJ, 751, L27
Weberg, M. J., Morton, R. J., & McLaughlin, J. A. 2018, ApJ, 852, 57
Weberg, M. J., Morton, R. J., & McLaughlin, J. A. 2020, ApJ, 894, 79
West, M. J., Zhukov, A. N., Dolla, L., & Rodriguez, L. 2011, ApJ, 730, 122
White, R. S. & Verwichte, E. 2012a, A&A, 537, A49
White, R. S. & Verwichte, E. 2012b, A&A, 537, A49
Withbroe, G. L. & Noyes, R. W. 1977, ARA&A, 15, 363
Zhong, S., Nakariakov, V. M., Kolotkov, D. Y., & Anfinogentov, S. A. 2022a, MNRAS, 513, 1834
Zhong, S., Nakariakov, V. M., Kolotkov, D. Y., Verbeeck, C., & Berghmans, D. 2022b, MNRAS, 516, 5989